PHYSICAL REVIEW B **84**, 121404(R) (2011)

# Strong enhancement of high-voltage electronic transport in chiral electrical nanotube superlattices

Jürgen Dietel[1] and Hagen Kleinert[1,2]

[1]*Institut für Theoretische Physik, Freie Universität Berlin, Arnimallee 14, D-14195 Berlin, Germany*

[2]*International Center for Relativistic Astrophysics Network (ICRANeT), Piazzale della Repubblica 1, I-10-65122, Pescara, Italy*

(Received 21 June 2011; published 9 September 2011)

We consider metallic carbon nanotubes with an overlying unidirectional electrical chiral (wave vector out of the radial direction, where the axial direction is included) superlattice potential. We show that for superlattices with a wave vector close to the axial direction, the electron velocity assumes the same value as for nanotubes without a superlattice. Due to an increased number of phonons with different momenta but lower electron-phonon scattering probabilities, we obtain a large enhancement of the high-voltage conductance and current sustainability in comparison with the nanotube without a superlattice.

DOI: 10.1103/PhysRevB.84.121404 PACS number(s): 73.50.Fq, 63.22.Gh, 73.21.Cd, 73.63.Fg

Depending on their chirality, carbon nanotubes (NTs) behave either as a semiconductor or a metal. In the first case, they offer an interesting alternative for building logical circuits. In the second case, they can be used as nanometer-sized metallic wires in logical circuits. This is particularly useful since they can sustain very high currents before breaking. At low voltages ($U \lesssim 0.17$ V) the effective electron scattering length at room temperature in metallic NTs is mainly governed by acoustical phonon and impurity scattering with a value of a few hundred nanometers.[1] At higher voltages, scattering with hot optical phonons created by electron-phonon scattering becomes relevant. This leads to a significant reduction of the electron's mean free path down to roughly $l_{sc} \approx 10$ nm,[2–6] resulting in a large increase in the absolute and differential resistance. Due to the large number of optical phonons, phonon-phonon scattering with acoustic phonons produces heat in the NT that ultimately causes the electrical breakdown.[7,8]

In Ref. 9 it was argued that the performance of a metallic NT, i.e., its absolute and differential conductance, can be enhanced considerably by isotopical disorder enrichment. This causes additional relaxation paths for optical phonons by disorder scattering. The purpose of the present Rapid Communication is to propose a different mechanism to enhance the electronic transport. We show that by applying an unidirectional electrical superlattice (SL) (cf. Fig. 1) with a wave vector that is close to the axial direction of the NT, we can enhance the (differential) conductance considerably, especially in the large voltage regime. Such a potential could be, for example, produced by adatom deposition via electron beams directed on the NT[10] or (at least approximately) by twisted periodical patterned top and bottom gate electrodes or coupling of the NT to surface acoustic waves.[11] Since the (average) phonon number is proportional to the inverse electron-phonon scattering time $1/\tau_{ep}$, and the inverse electron mean free path $1/l_{sc}$ is proportional to the phonon number times $1/\tau_{ep}$ in the hot phonon regime, we obtain a quadratic dependence of the electron mean free path on the scattering time $l_{sc} \sim \tau_{ep}^2$. Below it will be shown that an application of an electrical chiral potential causes a large number of different phonons to take part in the electron-phonon scattering process with increased electron-phonon scattering times, so that $1/\tau_{ep} \sim \sum_i 1/\tau_{ep}^i$. This is what causes the strong decrease of the (differential) resistance that scales with $1/l_{sc} \sim \sum_i 1/(\tau_{ep}^i)^2 \ll 1/\tau_{ep}^2$ by using Matthiessen's rule and reduces the phonon temperature.

It was shown recently that new Dirac points in the energy spectrum can be opened by imposing a SL on the graphene lattice.[12–16] This is also seen in NTs for potentials with a wave vector in the radial direction. We will show that they vanish for general chiral potentials.

The Hamiltonian near the Dirac point **K** for a NT with an axis in the $y'$ direction subjected to a SL potential reads

$$H_K = \begin{pmatrix} V(x'+t_\gamma y') & -i\hbar v_F(\partial_{x'} - i\partial_{y'}) \\ -i\hbar v_F(\partial_{x'} + i\partial_{y'}) & V(x'+t_\gamma y') \end{pmatrix}, \tag{1}$$

where $v_F$ is the Fermi velocity. For a NT with circumference $D$, the SL potential $V$ is periodic in the radial (axial) direction with periodicity $d$ ($d/t_\gamma$), i.e., $V(x'+d) = V(x')$, and one has $D/d \in \mathbb{N}$. In the following we solve the eigenvalue equation $H_K\mathbf{u}(\mathbf{r}') = \epsilon\mathbf{u}(\mathbf{r}')$. We use the abbreviation $t_\gamma = \tan(\gamma)$, where $\gamma$ is the chiral angle of the SL potential $V$. The metallic NT boundary conditions are given by $\mathbf{u}(x'+D, y') = \mathbf{u}(x', y')$.[17]

To solve the eigenvalue equation we follow first a transfer matrix method similar to Ref. 14. By using the coordinates $x = x' + t_\gamma y'$ and $y = y'$, the solution of the Schrödinger equation has the Bloch form $\mathbf{u}(\mathbf{r}) = e^{iqy}[u_1(x), u_2(x)]^T$ with $[u_1(x), u_2(x)]^T = \Lambda(x)[u_1(0), u_2(0)]^T$, where

$$\Lambda(x) = e^{-i\tilde{q}x} P \exp\left[\int_0^x dx' M_{V(x')}\right], \tag{2}$$

$$M_{V(x)} = \begin{pmatrix} q/T_\gamma^2 & i\kappa(x)/(1+it_\gamma) \\ i\kappa(x)/(1-it_\gamma) & -q/T_\gamma^2, \end{pmatrix} \tag{3}$$

and $\tilde{q} = qt_\gamma/T_\gamma^2$, $\kappa(x) = [\epsilon - V(x)]/\hbar v_F$, $T_\gamma = \sqrt{1+t_\gamma^2}$. The operator $P$ indicates path ordering and places all larger values of $x$ to the left-hand side. The Bloch condition reads $[u_1(d), u_2(d)]^T = e^{i\eta}[u_1(0), u_2(0)]^T$ with $\det[e^{i\eta} - \Lambda(d)] = 0$ when $d$ is the SL wavelength.

Consider first a carbon NT in a chiral periodical lattice of two piecewise constant potentials of the form

$$V(x) = \begin{cases} V_1 & \text{if} \quad 0 \leqslant x < d_1, \\ V_2 & \text{if} \quad d_1 \leqslant x < d_1 + d_2. \end{cases} \tag{4}$$

 

Then we obtain $\Lambda(d) = \Lambda_1\Lambda_2$, where $d = d_1 + d_2$:

$$\Lambda_i = e^{-i\tilde{q}d_i}\left\{\cos[\alpha_\epsilon(d_i)] + \frac{\sin[\alpha_\epsilon(d_i)]}{\alpha_\epsilon(d_i)}M_{V_i}d_i\right\}, \quad (5)$$

$$\alpha_\epsilon(d_i) = d_i\sqrt{\kappa_i^2/T_\gamma^2 - q^2/T_\gamma^4}. \quad (6)$$

$\kappa_i$ is given by $\kappa(x)$, with $V(x) = V_i$. Since $\det[e^{i\tilde{q}x}\Lambda(x)] = 1$ we have for the eigenvalues of the matrix $\Lambda(d)$, $\xi = e^{-i\tilde{q}d}(1/2)(T \pm \sqrt{T^2-4})$, with $T = \mathrm{Tr}[e^{i\tilde{q}d}\Lambda(d)]$ and

$$T = 2\cos[\alpha(d_1)]\cos[\alpha(d_2)] + 2\frac{\sin[\alpha(d_1)]\sin[\alpha(d_2)]}{\alpha(d_1)\alpha(d_2)} \times \left(\frac{q^2}{T_\gamma^4} - \frac{\kappa_1\kappa_2}{T_\gamma^2}\right)d_1d_2. \quad (7)$$

By taking into account that $T$ is real, we obtain from (7) the dispersion relation

$$2\cos(\tilde{q}d + \eta) = T. \quad (8)$$

In the following, we restrict ourselves to the mirror symmetric potentials $V_1 = -V_2 = V$, with $d_1 = d_2 = d/2$ leading to the best current-voltage results over all two-step potentials. This leads to an energy spectrum that possesses a mirror symmetry at $\epsilon = 0$ as a function of the quasimomentum $q$ in the $y$ direction. For $\epsilon = 0$, we obtain from Eq. (8) that $T = 2 + q^2d^2\sin^2[\alpha_0(d/2)]/\alpha_0^2(d/2)T_\gamma^4$. This leads with (8) to the existence of new Dirac points[14] at zero chirality $t_\gamma = 0$. The number of these points is given by $[Vd/2\pi\hbar v_F T_\gamma]$, where $[x]$ is the largest integer number smaller than $x$. For $t_\gamma \neq 0$ an energy gap is opened and the Dirac points disappear (see the left-hand panel in Fig. 1).

Next we calculate the energy values of the bands at zero momentum $q = 0$. Equations (7) and (8) deliver for these energy values $\epsilon^\eta(0) = (\pm\eta + 2\pi n)T_\gamma\hbar v_F/d$, where $n$ determines the energy bands for fixed quasimomentum $\eta$. Thus the energy bands are far more separated in energy space for $t_\gamma \gg 1$ than for the system without a chiral potential, i.e., $\epsilon^\eta(0)$ for $t_\gamma = 0$.

In order to see how the lowest-energy band scales with $V$ and $t_\gamma$, we calculate from (7) the energy dispersion of the lowest band for metallic NTs, i.e., $\eta = 0$, in the regime $|\epsilon_s| \ll \hbar v_F T_\gamma/d$, $V$, and $q^2 \ll T_\gamma^2(V(x)/\hbar v_F)^2$, to be called $R$. We then obtain

$$\epsilon_s = s\hbar v_F\sqrt{\frac{|q\Gamma|^2}{T_\gamma^2} + 4\frac{T_\gamma^2}{d^2}\sin^2\left(\frac{\tilde{q}d}{2}\right)}, \quad (9)$$

$$\Gamma = \frac{1}{d}\int_0^d dx\exp\left[i2\int_0^x dx'\mathrm{sgn}[V(x')]\alpha_0(x')/x'\right], \quad (10)$$

where $s = \pm 1$ and $\mathrm{sgn}[x]$ is the sign of $x$. Note that $\Gamma = \sin[\alpha_0(d/2)]e^{i\alpha_0(d/2)}/\alpha_0(d/2)$ for the symmetric two-step potential (4).

In Fig. 1, we plot the two lowest-energy bands ($d = D$) for $\eta = 0$ by solving Eq. (8) numerically. Equation (9) leads to the electron velocity $v_{y'}(q) = \partial\epsilon_s/\partial(\hbar q)$ along the NT axis (the $q$ dependency of $\tilde{q}$ has to be considered in the derivate). We restrict our discussion to momentum region near the Dirac point, i.e., $\tilde{q}d/2 \ll 1$. It is smaller for larger potentials $V$ being maximal at $\alpha_0 \to 0$ with a value of $v_{y'}(q) \leqslant v_F$. We

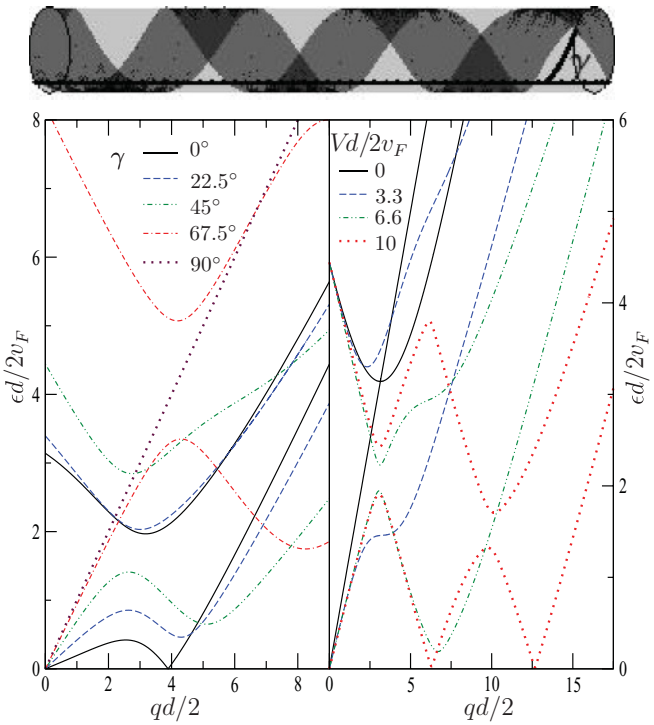


FIG. 1. (Color online) The upper panel shows a NT with an overlying chiral electrical superlattice potential. The lower panel shows the two lowest-energy bands ($d = D$) by solving Eq. (8) for $\eta = 0$ as a function of the rescaled axial quasimomentum $qd/2$ for various chiral angles $\gamma$ with $Vd/2\hbar v_F = 5$ (left-hand panel) and various chiral potentials $Vd/2\hbar v_F$ with $t_\gamma = 1$ (right-hand panel). Note that the dotted curve in the right-hand panel crosses the $x$ axis exactly only at $q = 0$.

point out that in general for $|t_\gamma| \gtrsim 1$ we have $v_{y'}(q) \approx v_F$ in $R$, irrespective of the potential strength $V$. Since electron-phonon scattering times are proportional to $v_{y'}(q)$ we restrict our transport calculations below to NTs with $|t_\gamma| \gtrsim 1$ leading to the largest conductivities. For the group velocity of the electrons in the radial direction we have $v_{x'}(q) = \partial\epsilon_s/\partial(\hbar\tilde{q}) - t_\gamma v_{y'}(q)$. For $t_\gamma \gtrsim 1$ we obtain $v_{x'} \approx v_F(1 - |\Gamma|^2)/T_\gamma$ in $R$, leading to the collimination of the electron beam,[18] i.e., $|v_{y'}(q)| > |v_{x'}(q)|$. This expression is even valid where $t^2 \gg |\Gamma|^2$. On the other hand, for $t^2 \ll |\Gamma|^2$ we obtain $v_{x'} \approx t_\gamma v_F(1 - |\Gamma|^2)/\Gamma$, leading to the vanishing of collimination at chiral angles $|\Gamma|^2/(1 - |\Gamma|^2) \lesssim |t_\gamma| \lesssim (1 - |\Gamma|^2)$. For even smaller $t_\gamma$ we obtain collimination again.

In Fig. 1 we see how the energy bands oscillate, in accordance with Eq. (9) for $q \leqslant T_\gamma V/\hbar v_F$, thus forming band SL valleys. The central valley possesses a true Dirac point at $q = 0$. The SL side valleys then have a minimum at $\sin^2(\tilde{q}d/2) = 0$. Within the SL valleys, electrons travel either to the left-hand side (right-hand side) for $\partial\epsilon_s/\partial q < 0$ ($\partial\epsilon_s/\partial q > 0$). The number of side valleys can be read of from (9) as $2m_1$ with $m_1 = [t_\gamma Vd/T_\gamma\hbar v_F 2\pi]$.

For SLs with a wave vector in an exact axial direction we can read off the physics from the chiral case by choosing $\tilde{q} \to k$, $t_\gamma = \eta = 0$, where $d$ is now the wavelength of the SL potential in the axial direction with quasimomentum $k$. The wave vector $q$ in the circumferential direction is quantized by $q = 2\pi n/D$ due to the periodic boundary conditions of

the wave functions. We point out that also the wave functions Eqs. (11) and (12), and the considerations below Eqs. (11) and (13) are still valid with the additional replacements $k_x \to k_y$ and $x \to y$. Equation (9) shows that the energy bands are separated by $\hbar v_F q\Gamma$, which means that the energy spacing between the energy bands goes to zero for infinite potential strength. From Eq. (9) we have $v \to v_F$ for $Vd/\hbar v_F \to \infty$, where for the lowest band, i.e., $q = 0$, $v \to v_F$ even for finite potentials $Vd/\hbar v_F$.

Next, we determine the eigenvectors $\mathbf{v}^\eta$ of the matrix $\Lambda(d)$. These are given by $\mathbf{v}^\eta = \frac{1}{N_\Lambda}([a + i\sin(\eta + \tilde{q}d)]/b, 1)^T$ with

$$a = \left[qd_2\cos(\alpha_1)\frac{\sin(\alpha_2)}{\alpha_2} + qd_1\cos(\alpha_2)\frac{\sin(\alpha_1)}{\alpha_1}\right]\frac{1}{T_\gamma^2},$$
$$b = \left[\kappa_2 d_2\cos(\alpha_1)\frac{\sin(\alpha_2)}{\alpha_2} + \kappa_1 d_1\cos(\alpha_2)\frac{\sin(\alpha_1)}{\alpha_1}\right]\frac{i}{1 - it_\gamma}$$
$$-i\frac{\sin(\alpha_1)\sin(\alpha_2)}{\alpha_1\alpha_2}\frac{d_1 d_2 q(\kappa_1 - \kappa_2)}{T_\gamma^2(1 - it_\gamma)}, \tag{11}$$

and $N_\Lambda$ is a normalization factor. The eigenfunction $\mathbf{u}^\eta(x,q)$ of the full Hamiltonian $H_K$ is then given by $\mathbf{u}^\eta(x,q) = (\cos[\alpha_0(x)]I + \{\sin[\alpha_0(x)]/\alpha_0(x)\}M_V)\mathbf{v}^\eta$ for $x < d/2$. Equation (11) leads to $\langle\mathbf{u}^\eta(x,q)|e^{ik_x x}I|\mathbf{u}^{-\eta}(x,-q)\rangle = 0$, where we used the abbreviation $\langle\mathbf{u}^\eta(x,q)|e^{ik_x x}\sigma|\mathbf{u}^{-\eta}(x,-q)\rangle \equiv \int_0^d dx\langle\mathbf{u}^\eta(x,q)|e^{ikx}\sigma|\mathbf{u}^{-\eta}(x,-q)\rangle$ with $\sigma \in \{\sigma_x,\sigma_y,I\}$. Here $I$ is the identity matrix and $\sigma_x$,$\sigma_y$ are the spin matrices. The wave vector of the phonons or impurities is denoted by $k_x$. This is a generalization of the results that inner-valley backward impurity scattering in Refs. 19 and 20 and deformation potential phonon scattering in Ref. 21 does not exist in the lowest band in metallic NTs in contrast to semiconducting ones.

We then obtain from (11) for the lowest band eigenfunctions $\mathbf{u}_s(x,q)$ for $\eta = 0$ in the regime $R$ corresponding to the eigenvalues (9)

$$\mathbf{u}_s(x,q)$$
$$= \frac{1}{N_u}e^{-i\tilde{q}x}\left[-i\left(\frac{\sqrt{1-it_\gamma}}{\sqrt{1+it_\gamma}}\right)\frac{T_\gamma}{\Gamma^*}\times\left(\frac{T_\gamma}{qd}\sin(\tilde{q}d) + \frac{\epsilon_s}{\hbar v_F q}\right)\right.$$
$$\left.\times\phi^*(x) + \begin{pmatrix}-\sqrt{1-it_\gamma}\\ 1+it_\gamma\end{pmatrix}\phi(x)\right], \tag{12}$$

where $N_u$ in (12) denotes a normalization factor. The phase factor $\phi(x)$ is given by $\phi(x) = \exp[i\int_0^x dx'\mathrm{sgn}[V(x')]\alpha_0(x')/x']$. We point out that the lowest band eigenvalues (9) and eigenfunctions (12) are more generally valid for chiral potentials $V(x) = V(x + D)$, where we have to assume that $\int_0^D dx'\,\mathrm{sgn}[V(x')]\alpha_0(x')/x' = 0$. In order to derive the eigenfunctions (12) we first formulate the eigenvalue problem corresponding to (1) in the basis $(\sqrt{1-it_\gamma},\sqrt{1+it_\gamma})^T e^{-i\tilde{q}x}\phi^*(x)e^{iqy}$ and $(-\sqrt{1-it_\gamma},\sqrt{1+it_\gamma})^T e^{-i\tilde{q}x}\phi(x)e^{iqy}$. The resulting Hamiltonian is evaluated perturbatively in lowest order in $(\hbar v_F/d)T_\gamma\sin(\tilde{q}d)\sigma_z$ and $(\hbar v_F q/T_\gamma)\{(\mathrm{Re}[\phi^2(x)]\sigma_y + \mathrm{Im}[\phi^2(x)]\sigma_x\}$, resulting in (9) and (12) when the $\sim q^2$ terms in $\alpha_0$ are absent. The full expressions (9) and (12) valid in the regime $R$ can then be read off by comparing the first-order expressions with the formal solution of (8) for general chiral potentials $V(x)$, leading effectively to the $\sim q^2$ correction factor in $\alpha_0$ (6).

By using (12) we are now able to calculate the backward squared transition matrix elements in the regime $R$ being inverse proportional to the inverse electron-phonon scattering time. Here we restrict ourselves to SL inner- and intervalley backward scattering, i.e., $\partial_q\sin(\tilde{q}d/2)^2 \gtrless 0$ and $\partial_{q'}\sin(\tilde{q}'d/2)^2 \lessgtr 0$, at large chiral angle $|t_\gamma| \gtrsim 1$, for $(qd)^2\Gamma^2 \ll 4T_\gamma^4\sin(\tilde{q}d/2)^2$ and $(q'd)^2\Gamma^2 \ll 4T_\gamma^4\sin(\tilde{q}'d/2)^2$, which is the relevant regime for transport at high applied bias voltages. We obtain

$$|\langle\mathbf{u}_s(x,q)|\sigma e^{ik_x x}|\mathbf{u}_{s'}(x,q')\rangle|^2$$
$$\approx (A_\sigma^0)^2\delta_{\tilde{k}_x d,0} + \frac{1}{2m_2}(A_\sigma^1)^2\sum_{j=1}^{m_2}\sum_{\pm}\delta_{\tilde{k}_x d,\pm 2\pi[2V_j d/2\pi\hbar v_F T_\gamma]}, \tag{13}$$

where $(A_\sigma^0)^2 \approx 0$ and $(A_{\sigma_x}^1)^2 \approx 1$, $(A_{\sigma_y}^1)^2 \approx (A_I^1)^2 \approx 0$. Here we introduced the abbreviation $\tilde{k}_x = k_x - \tilde{q}' + \tilde{q}$. Note that we used in (13) the approximation that $\alpha_0(d_i) \approx d_i|V_i|/\hbar v_F T_\gamma$, which is valid for the majority of SL valleys.

For the symmetric two-step potential (4) we have $m_2 = 1$ and $V_1 = V$ in (13). We generalized in (13) our results to a chain of symmetric two-step potentials with $d_1 = d_2 = d/2m_2$ of potential heights $V_i$, where we assume the potential heights are separated considerably $[2V_i d/2\pi\hbar v_F T_\gamma] \neq [2V_j d/2\pi\hbar v_F T_\gamma] \neq 0$ for $i \neq j$. This restriction implies that the number of different phonons taking part in an electron-phonon scattering process is maximal. Equation (13) shows that for every phonon type of a certain momentum the scattering probability is $1/2m_2$ smaller than in the case of no existing chiral potential.[6] By using (12) we obtain, for general step potentials within the same approximation used in (13), $\sum_{k_x}|\langle\mathbf{u}_s(x,q)|\sigma e^{ik_x x}|\mathbf{u}_{s'}(x,q')\rangle|^2 \approx 1$ for $\sigma = \sigma_x$ and zero for $\sigma \in \{\sigma_y,I\}$. This shows, with the help of the discussion above, that the considered chain of symmetric two-step potentials (13) should give the best transport results over all step potentials and that even a general step potential should show an enhanced conductivity when compared to the pristine NT.

The number of SL valleys for a chain of two-step potentials is now $m_1 = [|t_\gamma|\min[V_i]d/T_\gamma\hbar v_F 2\pi]$, which can be read off from Eqs. (5) and (6) as in the case of the symmetric two-step potential. Here we denote $\min[V_i]$ as the minimum of all $V_i$'s. Finally, we mention that for the forward scattering amplitudes, i.e. $\partial_q\sin(\tilde{q}d/2)^2 \gtrless 0$ and $\partial_{q'}\sin(\tilde{q}'d/2)^2 \gtrless 0$, we have $(A_{\sigma_y}^0)^2 \approx (A_I^0)^2 \approx 1$, $(A_{\sigma_x}^0)^2 \approx 0$ and $(A_\sigma^1)^2 \approx 0$ in (13).

Until now, we have ignored transitions of electrons between the $\mathbf{K}$ and $\mathbf{K}'$ valleys. For the eigenvalue problem of the $\mathbf{K}'$ valley we can repeat the discussion above for the $\mathbf{K}$ valley by using the substitution $t_\gamma \to -t_\gamma$ and $q \to -q$ in the corresponding expressions.[21] Zone boundary $A_1'$ phonon backward scattering is the only relevant phonon-scattering mechanism in this case.[5,6] We now have to calculate the square of transition matrix element (13) with $\sigma = \sigma_y$,[22] where one of the wave functions stands for a $\mathbf{K}'$ valley function and the other is an eigenfunction of the $\mathbf{K}$ valley. Equation (13) leads to $(A_{\sigma_y}^0)^2 \approx 0$ and $(A_{\sigma_y}^1)^2 \approx 1$. The corresponding forward scattering amplitudes vanish.

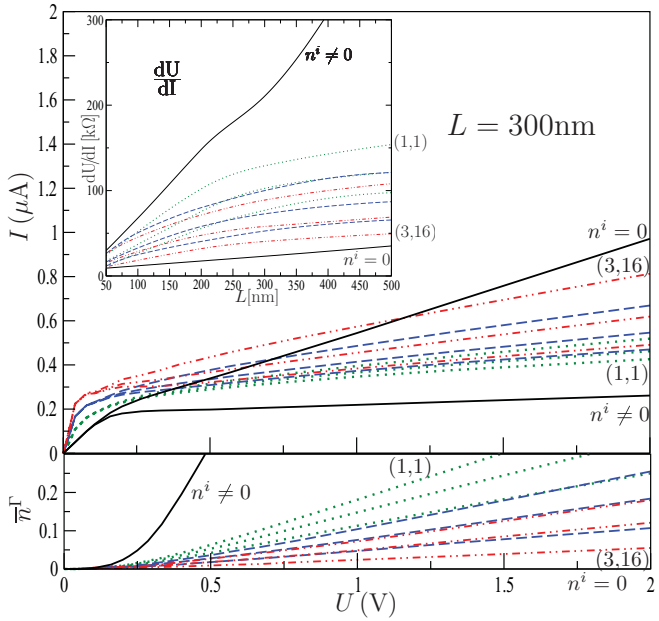


FIG. 2. (Color online) Upper panel: Current-voltage characteristic of the $(m_1,m_2)$ model ($2m_1$ SL side valleys and $2m_2$ phonon species) for $m_1 = 1$ (green dotted curves), $m_1 = 2$ (blue dashed curves), and $m_1 = 3$ (red dashed-dotted curves). Curves of the same style have different $m_2$ parameters with $(m_1,1)$ (bottom curves), $(m_1,m_1+1)$ (middle curves), and $(m_1,(m_1+1)^2)$ (top curves). This ordering is reversed in the inset and in the lower panel. The NT length is $L = 300$ nm. The black solid curves show the current-voltage characteristic with zero chiral potential $V = 0$ and hot phonons ($n^i \neq 0$) or frozen phonons fixed at zero temperature ($n^i = 0$) (Ref. 6). Inset: Differential resistance as a function of the NT length $L$. Lower panel: Position and energy-averaged phonon number of SL inner-valley $\Gamma$ phonons $\overline{n}^\Gamma$ for $L = 300$ nm (Ref. 6).

Let us now consider the conductance of a NT with a SL potential. To this end we use the electron-phonon Boltzmann approach with the parameters established in Refs. 5, 6, and 23 for a NT lying on a substrate without a chiral potential, where also thorough discussions on the scattering mechanisms can be found. The leads and the substrate are fixed at room temperature. Before going into the details of our calculation we want to recall here that the number $2m_1$ was defined as the number of the SL side valleys and $2m_2$ is the number of steps in the SL chain potential which is equal to the number of different phonon species taking part in a backward scattering process.

In the following, we assume that higher bands do not contribute to the conductivity, so that we have $\hbar v_F T_\gamma 2\pi/D \gtrsim eU$ ($\hbar v_F 2\pi/d \gtrsim eU$) for wave vectors of the SL out of (exact in) axial direction. For large enough applied bias voltages $eU \gg |\epsilon_s(q_i)|$, where $q_i$ is defined by $\sin(\tilde{q}_i d/2) = 0$, $q_i^2 \ll T_\gamma^2(\min[V_j]d/\hbar v_F)^2$, and large chirality, i.e., $t_\gamma \gtrsim 1$, we obtain the following idealized band system: We have one central SL band with dispersion $\epsilon(k) \approx \pm\hbar v_F|k|$ and $2m_1$ SL sidebands with a momentum-shifted dispersion $\epsilon(k) \approx \pm\lim_{k_0\to 0}\hbar v_F\sqrt{k^2+k_0^2}$. Phonons of $2m_2$ type contribute to electron-phonon backward scattering with scattering times $2m_2\tau_{\mathrm{ep}}^\nu$. Here $\nu$ stands for $\Gamma$ for longitudinal $E_2$ zone-center scattering or $K$ for $A_1'$ zone-boundary phonon scattering.[5,6] $\tau_{\mathrm{ep}}^\nu$ is the corresponding electron-phonon scattering time without a chiral potential. We can simplify our calculation by using the same phonon velocity $v_{\mathrm{op}}^\nu$ (Refs. 5 and 6) of the system without SL for all types of optical phonons. This is justified by the fact that our results do not depend much on the specific velocity value since the phonon mean free path is much smaller than the NT length, as we have verified numerically.

It is enough to consider only forward scattering between the central SL valley and the $2m_1$ side valleys mediated by transversal optical $\Gamma$ phonons with a scattering time $\tau_{\mathrm{ep}}^\Gamma$,[6] where we use calculation methods established in Ref. 23 for forward scattering. At low voltages $U \lesssim 0.17$ V, quasielastic scattering is relevant and we take it into account in our numerical calculations by inner SL valley scattering. This approximation is exact for voltages lower than the SL side-valley energy gap. We can simplify even further the model to an effective two-valley model with one central SL valley and one side valley by using the approximation of periodic boundary conditions for the positions of the potential valleys in momentum space.

In Fig. 2, we show our results for the conductance, the differential conductance, and the position and energy-averaged phonon number $\overline{n}_\Gamma$ for certain $(m_1,m_2)$ values and lengths $L$. Here $n_\Gamma$ mediates the inner SL valley scattering. Note that an upper limit for $2m_1$, $2m_2$ is given by the number of excitable circumferential phonons, i.e., $2m_1,\ 2m_2 \lesssim d/\sqrt{3}a$ where $a$ is the NT interatomic distance $a \approx 1.42$ Å. We obtain a strong increase in the absolute conductance and differential conductance at high voltages ($U \approx 2$ V) as a function of $m_1$ and $m_2$ while $\overline{n}_\Gamma$ is strongly decreasing. The reason for an increase of the conductance for larger $m_1$ values and fixed $m_2$ comes mainly from the fact that, due to the band edges of the side valleys, scattering from the central SL valley to the SL side valleys is effectively forward. The backscattering to the central valley is accomplished then by a number of different phonons in contrast to the system without a chiral potential. The growth of the conductance as a function of $m_1$ is then seen from our discussion above, which also leads to the explanation of the conductance increase as a function of $m_2$.

Summarizing, we have shown that large chiral unidirectional superlattice potentials in metallic NTs should lead to a large increase of the conductance, the differential conductance, and to a decrease of the optical phonon temperature at high voltage. We have shown this explicitly for a chainlike SL potential with symmetric steps. This kind of SL potential leads to the best transport results over all step potentials. Nevertheless, the main effect should be also observed for at least other SL step potentials with strong chirality. The effect arises from an increased number of phonons with different momenta but lower electron-phonon scattering probabilities contributing to the electron-phonon scattering process. As a result of our findings, we expect an increase of the applicability of carbon NTs as metallic wires.

[1]M. S. Purewal, B. H. Hong, A. Ravi, B. Chandra, J. Hone, and P. Kim, Phys. Rev. Lett. **98**, 186808 (2007).
[2]Z. Yao, C. L. Kane, and C. Dekker, Phys. Rev. Lett. **84**, 2941 (2000).
[3]J. Y. Park, S. Rosenblatt, Y. Yaish, V. Sazonova, H. stnel, S. Braig, T. A. Arias, P. W. Brouwer, and P. L. McEuen, Nano Lett. **4**, 517 (2004).
[4]A. Javey, J. Guo, M. Paulsson, Q. Wang, D. Mann, M. Lundstrom, and H. Dai, Phys. Rev. Lett. **92**, 106804 (2004).
[5]M. Lazzeri and F. Mauri, Phys. Rev. B **73**, 165419 (2006).
[6]J. Dietel and H. Kleinert, Phys. Rev. B **82**, 195437 (2010).
[7]P. G. Collins, M. Hersam, M. Arnold, R. Martel, and P. Avouris, Phys. Rev. Lett. **86**, 3128 (2001).
[8]J. Y. Huang, S. Chen, S. H. Jo, Z. Wang, D. X. Han, G. Chen, M. S. Dresselhaus, and Z. F. Ren, Phys. Rev. Lett. **94**, 236802 (2005).
[9]N. Vandecasteele, M. Lazzeri, and F. Mauri, Phys. Rev. Lett **102**, 196801 (2009).
[10]J. C. Meyer, C. O. Girit, M. F. Crommie, and A. Zettl, Appl. Phys. Lett. **92**, 123110 (2008).
[11]V. I. Talyanskii, D. S. Novikov, B. D. Simons, and L. S. Levitov, Phys. Rev. Lett. **87**, 276802 (2001).
[12]C.-H. Park, Y. W. Son, L. Yang, M. L. Cohen, and S. G. Louie, Phys. Rev. Lett. **103**, 046808 (2009).
[13]L. Brey and H. A. Fertig, Phys. Rev. Lett. **103**, 046809 (2009).
[14]D. P. Arovas, L. Brey, H. A. Fertig, E.-A. Kim and K. Ziegler, New J. Phys. **12**, 123020 (2010).
[15]M. Barbier, P. Vasilopoulos, and F. M. Peeters, Phys. Rev. B **80**, 205415 (2009).
[16]Li-Gang Wang and Shi-Yao Zhu, Phys. Rev. B **81**, 205444 (2010).
[17]H. Ajiki1 and T. Ando, J. Phys. Soc. Jpn. **62**, 1255 (1993).
[18]C.-H. Park, Y.-W. Son, L. Yang, M. L. Cohen, and S. G. Louie, Nano Lett. **8**, 2920 (2008).
[19]T. Ando and T. Nakanishi, J. Phys. Soc. Jpn. **67**, 1704 (1998).
[20]P. L. McEuen, M. Bockrath, D. H. Cobden, Y. G. Yoon, and S. G. Louie, Phys. Rev. Lett. **83**, 5098 (1999).
[21]H. Suzuura and T. Ando, Phys. Rev. B **65**, 235412 (2002).
[22]H. Suzuura and T. Ando, J. Phys. Soc. Jpn. **77**, 044703 (2008).
[23]J. Dietel and H. Kleinert, Phys. Rev. B **83**, 245411 (2011).